NASA/TM—2009-215644

A Very Large Eddy Simulation of the Nonreacting Flow in a Single-Element Lean Direct Injection Combustor Using PRNS With a Nonlinear Subscale Model

Tsan-Hsing Shih
Ohio Aerospace Institute, Brook Park, Ohio

Nan-Suey Liu
Glenn Research Center, Cleveland, Ohio

August 2009

NASA STI Program . . . in Profile

Since its founding, NASA has been dedicated to the advancement of aeronautics and space science. The NASA Scientific and Technical Information (STI) program plays a key part in helping NASA maintain this important role.

The NASA STI Program operates under the auspices of the Agency Chief Information Officer. It collects, organizes, provides for archiving, and disseminates NASA's STI. The NASA STI program provides access to the NASA Aeronautics and Space Database and its public interface, the NASA Technical Reports Server, thus providing one of the largest collections of aeronautical and space science STI in the world. Results are published in both non-NASA channels and by NASA in the NASA STI Report Series, which includes the following report types:

- TECHNICAL PUBLICATION. Reports of completed research or a major significant phase of research that present the results of NASA programs and include extensive data or theoretical analysis. Includes compilations of significant scientific and technical data and information deemed to be of continuing reference value. NASA counterpart of peer-reviewed formal professional papers but has less stringent limitations on manuscript length and extent of graphic presentations.

- TECHNICAL MEMORANDUM. Scientific and technical findings that are preliminary or of specialized interest, e.g., quick release reports, working papers, and bibliographies that contain minimal annotation. Does not contain extensive analysis.

- CONTRACTOR REPORT. Scientific and technical findings by NASA-sponsored contractors and grantees.

- CONFERENCE PUBLICATION. Collected papers from scientific and technical conferences, symposia, seminars, or other meetings sponsored or cosponsored by NASA.

- SPECIAL PUBLICATION. Scientific, technical, or historical information from NASA programs, projects, and missions, often concerned with subjects having substantial public interest.

- TECHNICAL TRANSLATION. English-language translations of foreign scientific and technical material pertinent to NASA's mission.

Specialized services also include creating custom thesauri, building customized databases, organizing and publishing research results.

For more information about the NASA STI program, see the following:

- Access the NASA STI program home page at *http://www.sti.nasa.gov*

- E-mail your question via the Internet to *help@sti.nasa.gov*

- Fax your question to the NASA STI Help Desk at 443–757–5803

- Telephone the NASA STI Help Desk at 443–757–5802
- Write to:
  NASA Center for AeroSpace Information (CASI)
  7115 Standard Drive
  Hanover, MD 21076–1320

NASA/TM—2009-215644

A Very Large Eddy Simulation of the Nonreacting Flow in a Single-Element Lean Direct Injection Combustor Using PRNS With a Nonlinear Subscale Model

Tsan-Hsing Shih
Ohio Aerospace Institute, Brook Park, Ohio

Nan-Suey Liu
Glenn Research Center, Cleveland, Ohio

National Aeronautics and
Space Administration

Glenn Research Center
Cleveland, Ohio 44135

August 2009

Acknowledgments

Dr. T.-H. Shih is supported by the NASA Glenn Research Center NRA Program. The authors would like to thank Dr. Farhad Davoudzadeh for the numerical grid used in this study.

This report is a formal draft or working paper, intended to solicit comments and ideas from a technical peer group.

This report contains preliminary findings, subject to revision as analysis proceeds.

This work was sponsored by the Fundamental Aeronautics Program at the NASA Glenn Research Center.

Level of Review: This material has been technically reviewed by technical management.

Available from

NASA Center for Aerospace Information
7115 Standard Drive
Hanover, MD 21076–1320

National Technical Information Service
5285 Port Royal Road
Springfield, VA 22161

Available electronically at http://gltrs.grc.nasa.gov

Contents

A Very Large Eddy Simulation of the Nonreacting Flow in a Single-Element Lean Direct Injection Combustor Using PRNS With a Nonlinear Subscale Model

Tsan-Hsing Shih
Ohio Aerospace Institute
Brook Park, Ohio 44142

Nan-Suey Liu
National Aeronautics and Space Administration
Glenn Research Center
Cleveland, Ohio 44135

Abstract

Very large eddy simulation (VLES) of the nonreacting turbulent flow in a single-element lean direct injection (LDI) combustor has been successfully performed via the approach known as the partially resolved numerical simulation (PRNS/VLES) using a nonlinear subscale model. The grid is the same as the one used in a previous RANS simulation, which was considered as too coarse for a traditional LES simulation. In this study, we first carry out a steady RANS simulation to provide the initial flow field for the subsequent PRNS/VLES simulation. We have also carried out an unsteady RANS (URANS) simulation for the purpose of comparing its results with that of the PRNS/VLES simulation. In addition, these calculated results are compared with the experimental data. The present effort has demonstrated that the PRNS/VLES approach, while using a RANS type of grid, is able to reveal the dynamically important, unsteady large-scale turbulent structures occurring in the flow field of a single-element LDI combustor. The interactions of these coherent structures play a critical role in the dispersion of the fuel, hence, the mixing between the fuel and the oxidizer in a combustor.

1.0 Introduction

The lean direct injection (LDI) injector is a liquid fuel injector developed to reduce aircraft emissions. Stable combustion is essentially completed within a short distance through rapid fuel and air mixing. This design also allows for many small fuel injectors integrated into modules facilitating different fuel staging strategies, such as the one shown in Figure 1. So far, experimental observations have not fully clarified the dynamics of the mixing and combustion processes occurring in these injectors, and numerical studies need to be conducted to achieve a better understanding of the underlying unsteady physics of the LDI combustor.

A very large eddy simulation using PRNS (PRNS/VLES) has been carried out for the nonreacting turbulent flow in a single element LDI combustor as the first step towards the simulation of, for example, a 3 by 3 injector module.

PRNS/VLES is based on the concept of temporal filtering to enable a grid-independent very large eddy simulation (Refs. 1, 2, 3, 4, and 5). In PRNS/VLES, the contents of both the resolved and unresolved turbulence are regulated by a "resolution control parameter" (RCP), which is related to the width of the temporal filter. At a given RCP (between 0.0 and 1.0), the resolved, very large scales of the turbulence are directly calculated, and the effects of the unresolved scales of the turbulence are modeled by a dynamic equation system. This approach leads to a unified simulation strategy for URANS, VLES, and LES by varying the value of the RCP in conjunction with the use of grids which adequately support the intended resolution contents stipulated by the selected value of the RCP.

Figure 1.—A 9-elements LDI module.

2.0 PRNS/VLES of a Single-Element LDI Combustor

PRNS/VLES was performed for a single-element LDI combustor to study the complex unsteady turbulent structures occurring in its flow field and to compare the calculated results with available experimental data. The subscale model used in this simulation is the nonlinear dynamic subscale model, which has been proven to be able to simulate flows at both low and high Reynolds numbers as well as flows with high swirling (Ref. 5).

2.1 Grid, Initial, and Boundary Conditions

2.1.1 Grid

Figure 2 depicts the computational domain, grid spacing and a snap shot of the flow. The numerical grid consists of unstructured hexahedral elements, and the total number of the elements is 862,000. This is a relatively coarse grid used in a previous RANS simulation (Ref. 6). Embedded in this figure are the instantaneous iso-surface of the zero axial velocity component colored by the effective subscale viscosity and six instantaneous stream lines emanating from the inlet of the injector, going through the converging-diverging nozzle, then passing through the combustion chamber. Figure 2 is a snapshot taken at the instant of the 90,000 time step.

2.1.2 Initial and Boundary Conditions

The initial flow field for the present PRNS/VLES simulation is the solution of a steady RANS simulation (see Section 4.0), and no extra random fluctuations are imposed. At the upstream inlet, the axial velocity, the temperature and the density are specified according to the experimental condition (Ref. 7). The outlet boundary condition facilitates the convection of pressure disturbances out of the computational domain (Ref. 4). A generalized wall function (Ref. 8) is applied to all of the wall boundaries.

2.1.3 Numerical Setting

The National Combustion Code (NCC, Ref. 9) is used in this study to perform PRNS/VLES. When conducting numerical simulations, it is always critical to try to minimize the artificially added numerical dissipations as long as the numerical stability can be maintained. For the present simulation, the following numerical parameters are set in the NCC code: the coefficient of the 2nd order dissipation = 0.0, the coefficient of the 4th order dissipation = 0.01, the initial gauge pressure pg = 0.0, the physical time-step =

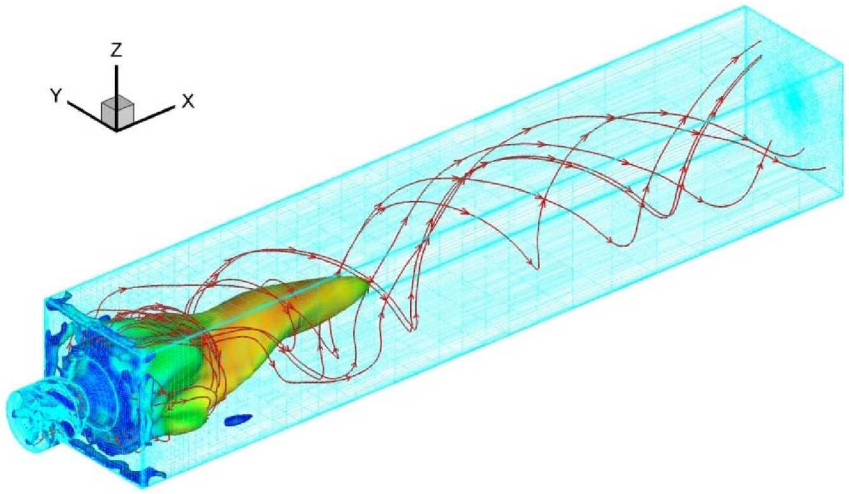

Figure 2.—Computational domain, grid spacing and a snap shot of the flow.

1.0E-06(s), the CFL number for the pseudo time iteration = 1.0, the convergence order for the pseudo time iteration = 2.0 or higher, and all of the residual smoothing parameters are 0.0.

In view of the grid resolution afforded by the present, relatively coarse grid, the value of RCP is set to 0.45. A more detailed discussion on the selection of the value of RCP can be found in Reference 5.

2.2 Numerical Results

The results of the present very large eddy simulation clearly demonstrate the presence of two interacting large scale turbulent structures in the flow field of the singe-element LDI combustor, namely, the precessing vortex core (PVC) and the vortex breakdown bubble (VBB). To illustrate the temporal variation of the flow field, the calculated instantaneous velocity profiles at 10 different instants (5000 time-steps apart) are shown, along with the experimentally determined time-mean profiles.

2.2.1 Contour Plots of Axial Velocity and Subscale k in the Center Plane

Figures 3 and 4 are the instantaneous contours of axial velocity u and subscale turbulent kinetic energy k in the center plane at the time-step of 90,000. Figure 3 shows that the strong recirculation zone has extended through the dump plane of the combustion chamber right up into the neighborhood of the injector tip which is located at the nozzle throat. Figure 4 shows that the subscale turbulent kinetic energy has high values inside the nozzle and in the neighborhood of the dump plane.

2.2.2 Contour Plots of Axial Velocity at the Combustor's Inlet and Outlet

Figure 5 is the instantaneous contour of the axial velocity at the dump plane of the combustion chamber, which indicates a strong upstream flow near the center. Figure 6 is the instantaneous contour of the axial velocity at the exit plane. In the center region, the axial velocity is lower due to the flow swirling.

2.2.3 Instantaneous PVC and VBB

The dominant flow structures in the LDI combustor can be best visualized via the iso-surface of the zero axial velocity and the iso-surface of a relatively low pressure (Ref. 10). The iso-surface of the zero axial velocity is also known as the vortex breakdown bubble (VBB). The iso-surface of a sufficiently low pressure captures the precessing vortex core (PVC). Figures 7 and 8 are the snap shots taken from two different angles. Figure 7 is a side view and Figure 8 is a perspective view. In these figures, the dark blue region is a vortex core, which is formed near the nozzle throat and extends into the combustor chamber. This spiraling vortex core rotates and breaks, it changes randomly in space and time. Embedded in these

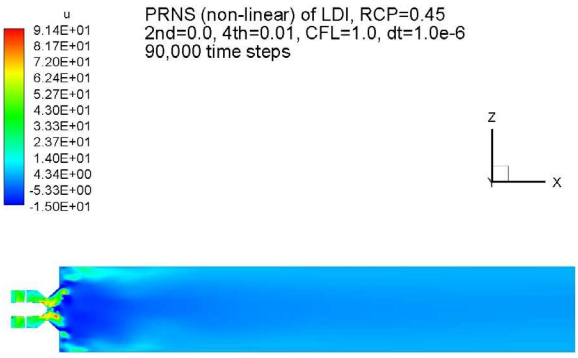

Figure 3.—Contour of axial velocity at center plane.

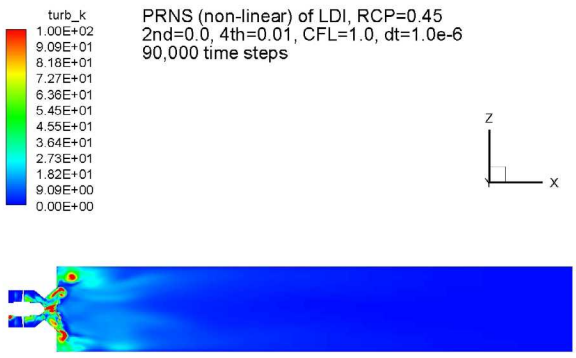

Figure 4.—Contour of k at center plane.

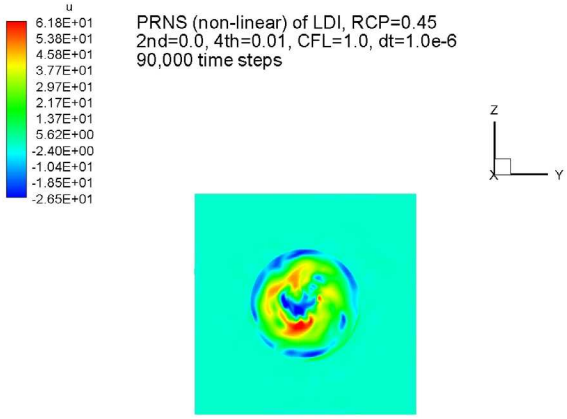

Figure 5.—Axial velocity at the dump plane.

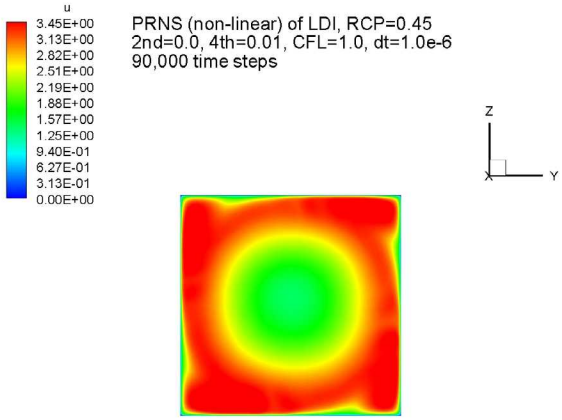

Figure 6.—Axial velocity at the exit plane.

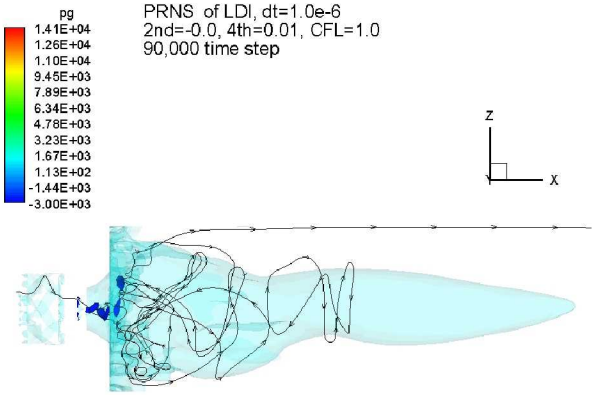

Figure 7.—PVC and VBB (side view).

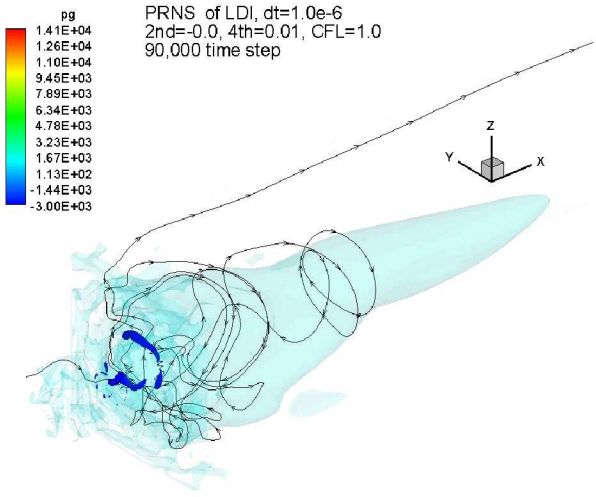

Figure 8.—PVC and VBB (a perspective view).

figures is an instantaneous stream line, which starts from the inlet of the injector and goes through a complex, seemingly random path in the combustor chamber. This stream line spirals around the dark blue surface indicating that the dark blue region is indeed a vortex core. The light green surfaces are the iso-surfaces of the zero axial velocity. In addition to the VBB, there are some small structures near the dump plane and in the corner region. It is very reasonable to expect that the dynamics of the PVC and the VBB, as well as their interactions, are critical to the fuel-air mixing and the flame stability in the LDI combustors.

2.2.4 Centerline Axial Velocity Profile

The instantaneous axial velocity profiles along the centerline from the nozzle throat (x = 0) to the exit of the combustor at ten different instants (5000 time-steps apart) are shown in Figure 9. The experimentally determined time-mean distribution is also given for reference. Figure 10 is an enlarged view near the dump plane of the chamber, which clearly shows significant variations of axial velocity component near the dump plane, and even much larger fluctuations in the upstream locations. This is consistent with the reported experimental observation that, close to the dump plane, the turbulent fluctuations are quite large.

2.2.5 Distribution of Axial Velocity Along the y-axis at Downstream Locations

The distributions of the axial velocity along the y-axis (i.e., z = 0) at several downstream locations (x = 3, 6, 9, 12, 15, and 90 mm) are presented for 10 different instants and compared with the experimental mean values. Figures 11, 12, and 13 clearly indicate that the turbulent fluctuations are quite large near the dump plane of the combustion chamber, and the fluctuations are quickly reduced towards downstream, as shown in Figures 14, 15, and 16. In addition, the largest turbulent fluctuations are off the centerline, somewhere between the centerline and the wall, which were also observed in the experimental studies.

2.2.6 Distribution of v, w Velocity Components Along the y-axis at Downstream Locations

The distributions of the other two velocity components v and w along the y-axis (i.e., z = 0) at several downstream locations (x = 3, 6, 9, 12, 15, and 90 mm) are shown for 10 different instants and compared with the experimental mean values in Figures 17 to 28. Again, these figures clearly indicate that the turbulent fluctuations are larger near the dump plane of the combustor chamber, and the fluctuations are quickly reduced towards downstream. The strongest turbulent fluctuations are found off the centerline, somewhere between the centerline and the wall.

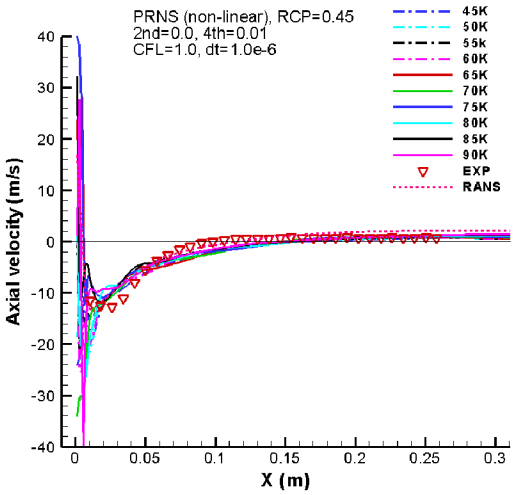

Figure 9.—Centerline axial velocity profile.

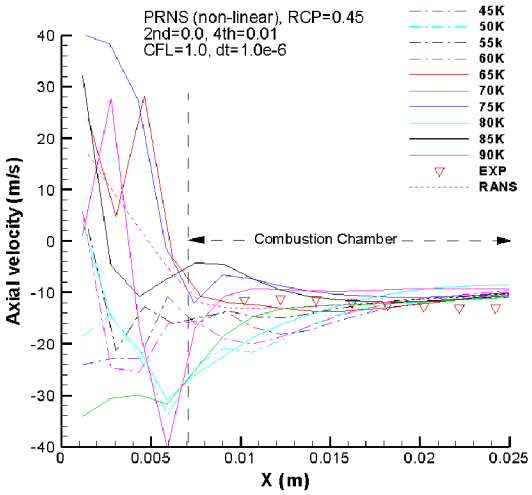

Figure 10.—Axial velocity near dump plane.

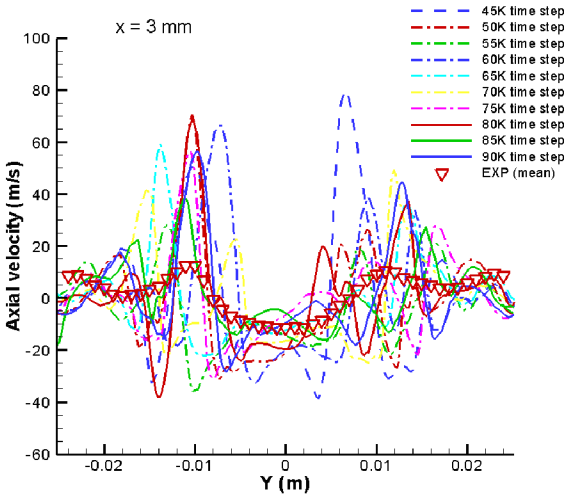

Figure 11.—Axial velocity at x = 3 mm.

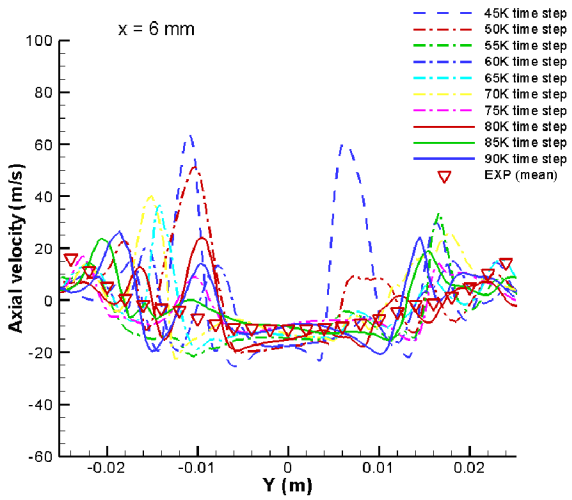

Figure 12.—Axial velocity at x = 6 mm.

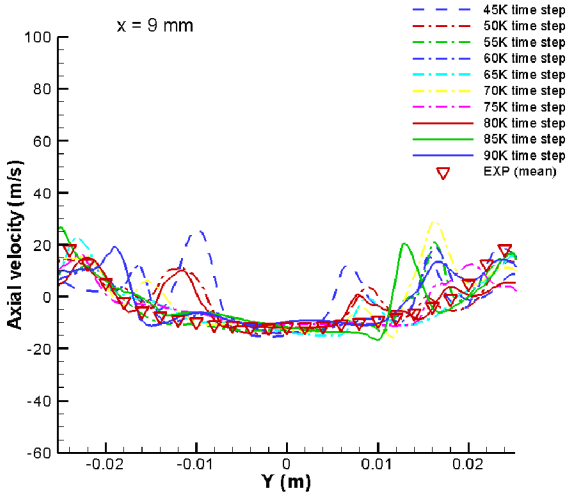

Figure 13.—Axial velocity at x = 9 mm.

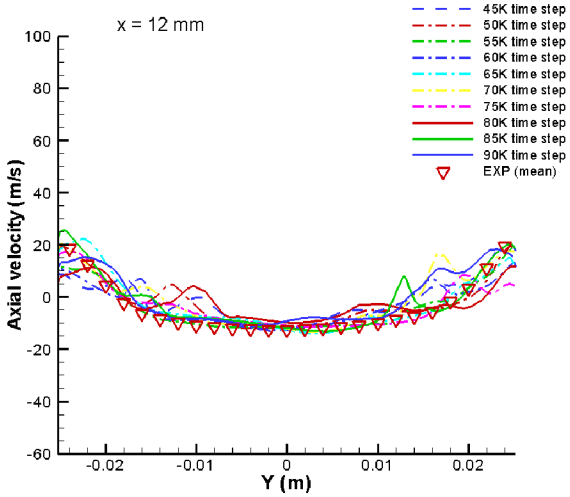

Figure 14.—Axial velocity at x = 12 mm.

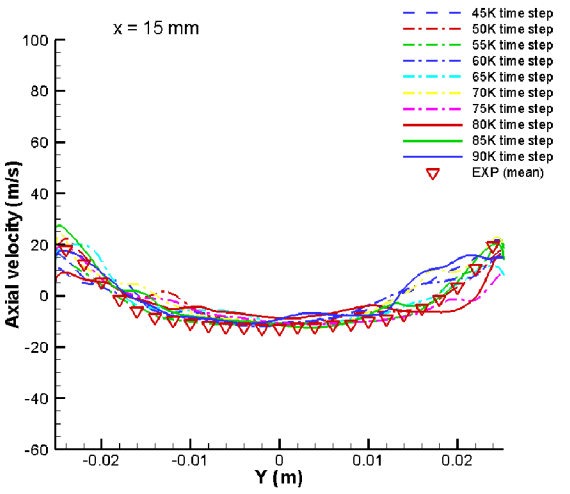

Figure 15.—Axial velocity at x = 15 mm.

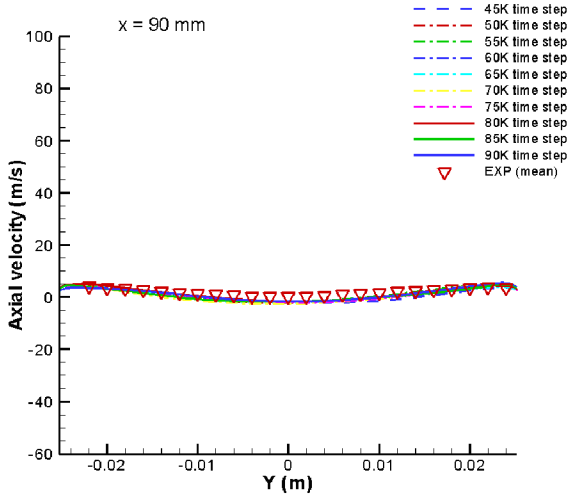

Figure 16.—Axial velocity at x = 90 mm.

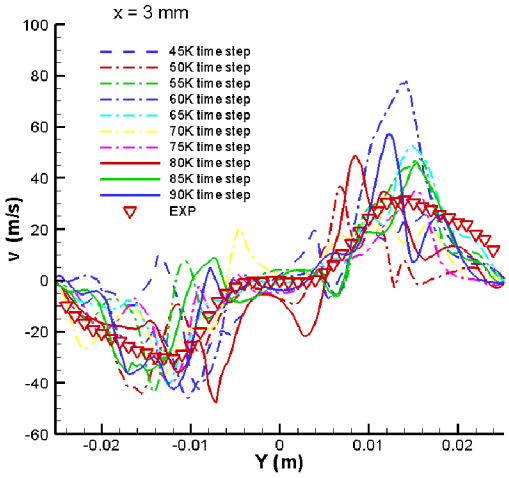

Figure 17.—Velocity component v at x = 3 mm.

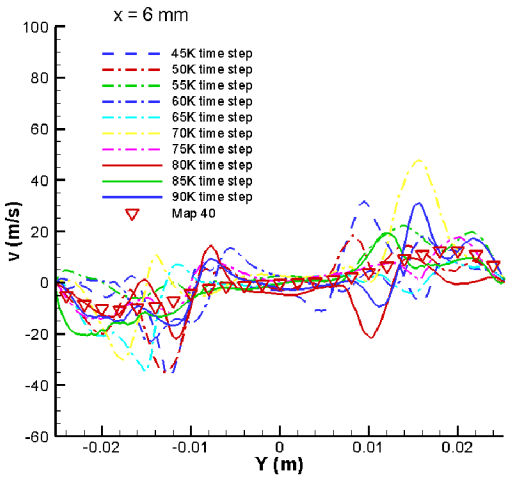

Figure 18.—Velocity component v at x = 6 mm.

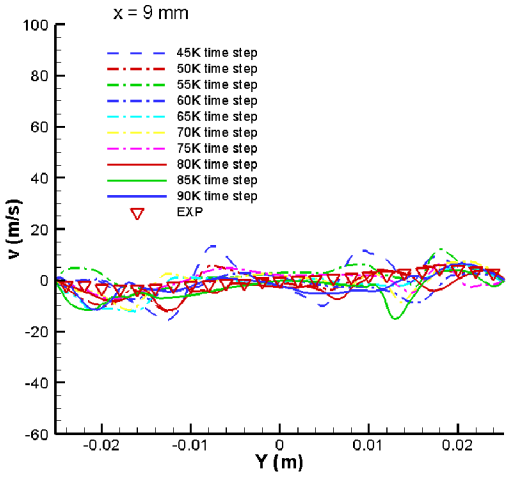

Figure 19.—Velocity component v at x = 9 mm.

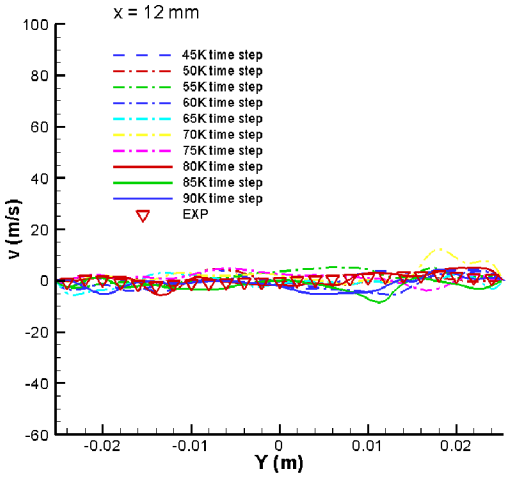

Figure 20.—Velocity component v at x = 12 mm.

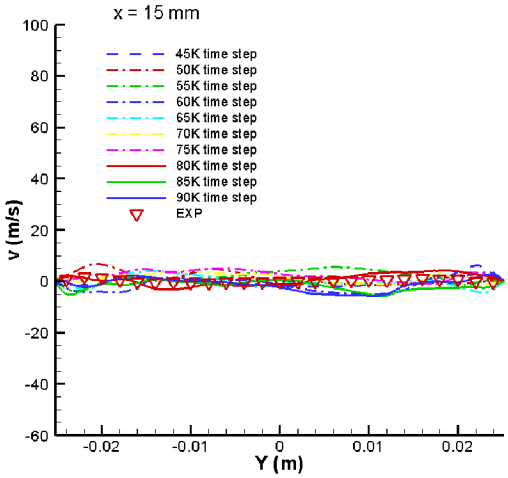

Figure 21.—Velocity component v at x = 15 mm.

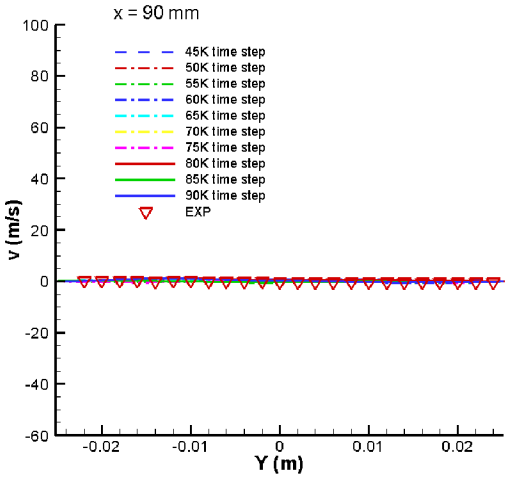

Figure 22.—Velocity component v at x = 90 mm.

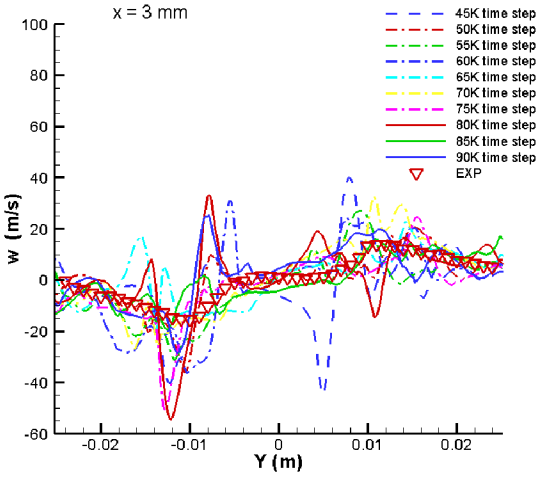

Figure 23.—Velocity component w at x = 3 mm.

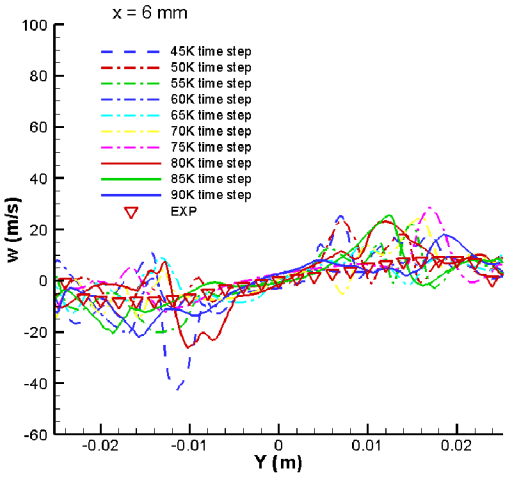

Figure 24.—Velocity component w at x = 6 mm.

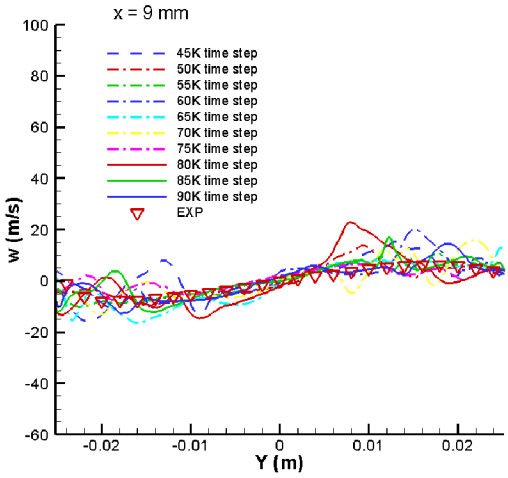

Figure 25.—Velocity component w at x = 9 mm.

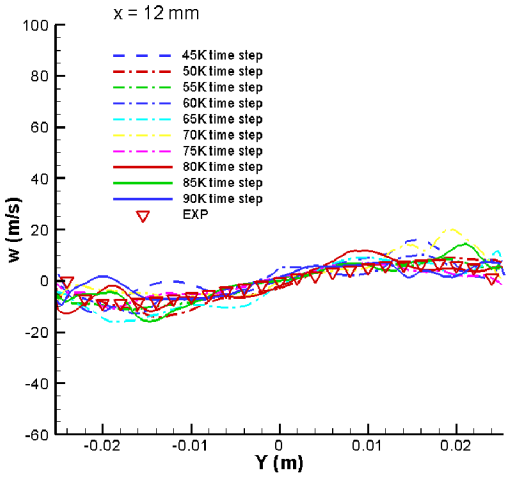

Figure 26.—Velocity component w at x = 12 mm.

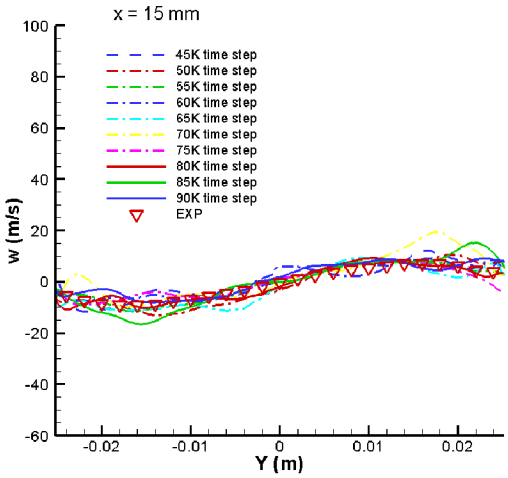

Figure 27.—Velocity component w at x = 15 mm.

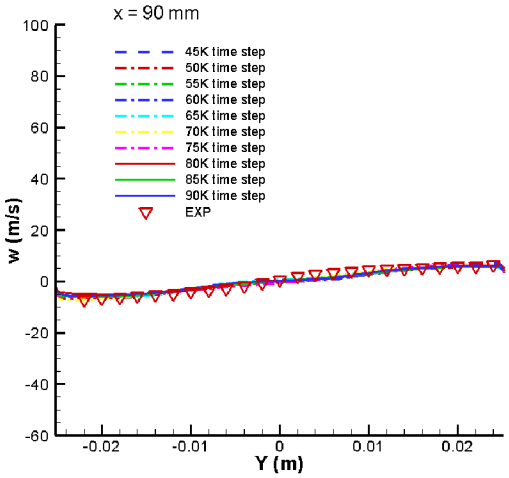

Figure 28.—Velocity component w at x = 90 mm.

2.3 Concluding Remarks

The numerical results presented above demonstrate that the very large eddy simulation of a complex turbulent flow in a single-element LDI combustor can be realized through the approach of PRNS/VLES using a coarse grid normally used in a RANS simulation. The dynamical behavior of the captured PVC and VBB is essentially the same as that revealed by a LES simulation that used about 2.2 millions grid points (Ref. 10). The 10 realizations of the instantaneous flow fields (5,000 time-steps apart) presented in Figures 11 to 28 closely fluctuate around the experimentally determined mean values, suggesting that PRNS/VLES results are also quantitatively meaningful.

3.0 URANS of a Single-Element LDI Combustor

An unsteady RANS (URANS) simulation is also performed for a single-element LDI combustor to elucidate the differences between the PRNS/VLES, the URANS and the RANS. In URANS, the turbulence model used is the nonlinear RANS model, but the temporal evolution of the flow field is calculated in a time-accurate manner, just like the PRNS/VLES.

3.1 Grid, Initial, and Boundary Conditions

The same computational domain and grid distribution shown in Figure 2 is used for the present URANS simulation. The boundary conditions are also the same as those used in the PRNS/VLES simulation (see Section 2.1.2). However, the initial condition for the URANS is a static flow field (an initial condition used for RANS in Section 4.0), i.e., the velocity is zero everywhere except for the upstream inflow boundary.

3.2 Numerical Results

When the value of the resolution control parameter RCP is 1.0, the PRNS/VLES equations become exactly the Reynolds averaged Navier-Stokes equations, and the subscale model of the PRNS/VLES becomes the traditional Reynolds stress model (see e.g., Ref. 5). Therefore, the result obtained by running PRNS/VLES with RCP = 1.0 is an URANS solution. Furthermore, the numerical setting in the NCC may be adjusted to reflect this change in the resolution content, i.e., we are now just dealing with the unsteady mean quantities of the turbulent flow, not including their fluctuations.

In the present URANS simulation, the following numerical parameters are set in the NCC code: the coefficient of the 2nd order dissipation = –0.02, the coefficient of the 4th order dissipation = 0.06, the initial gauge pressure pg = 0.0, the physical time-step = 1.0E-04(s), the CFL number for the pseudo time iteration = 1.0, the convergence order for the pseudo time iteration = 1.0 or higher, and all of the residual smoothing parameters are 0.0.

The temporal evolution of the calculated flow field reaches the asymptotic steady state at about the 50,000th time step. To verify the steadiness, the time accurate integration has been continued to the 90,000th time step; very little changes in the solutions have been observed.

3.2.1 Contour Plots of Axial Velocity and Turbulent Kinetic Energy in the Center Plane

Figures 29 and 30 are the contours of the axial velocity u and the turbulent kinetic energy k in the center plane. They are the snap shots taken at the time step 90,000. Figure 29 shows a steady recirculation zone extending through the dump plane of the combustion chamber into the upstream nozzle throat. Figure 30 shows that, in the diverging nozzle and near the dump plane, the turbulent kinetic energy k is quite high.

Figure 29.—Contour of axial velocity in center plane.

Figure 30.—Contour of k in center plane.

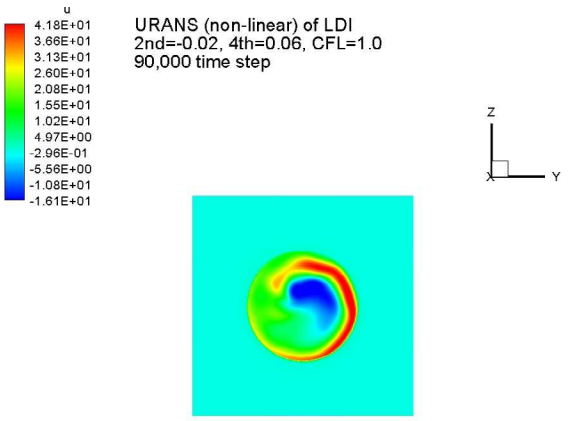

Figure 31.—Axial velocity at dump plane of combustor.

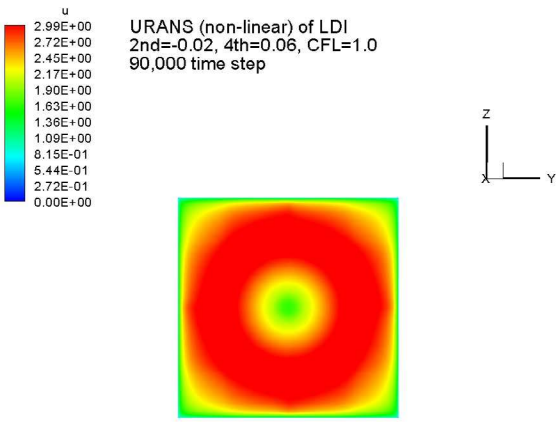

Figure 32.—Axial velocity at exit plane.

3.2.2 Contour Plots of Axial Velocity at the Combustor's Inlet and Outlet

Figure 31 is the contour of the axial velocity at the dump plane, which shows an asymmetric distribution of the axial velocity and a strong reverse flow off the center. Figure 32 is the contour of the axial velocity at the exit plane. The lower axial velocity region around the center is typical for flow with swirling.

3.2.3 PVC and VBB

For the purpose of comparing the characteristic flow structures captured by the URANS simulation with that captured by the PRNS/VLES simulation, we keep using the term PVC for the iso-surface of a relatively low pressure, and the term VBB for the iso-surface of the zero axial velocity, even now these URANS structures are time invariant. Figure 33 presents the side view, and Figure 34 presents the perspective view. In these figures, the "PVC" is a short blue stick, its location and shape do not change with the time, and it does not line up with the centerline of the nozzle. This may explain why the distribution of the axial velocity at the dump plane is asymmetric. The VBB is the light green surface, which is quite smooth and, by and large, axisymmetric. It is the familiar central recirculation zone (CRZ).

3.2.4 Centerline Axial Velocity Profile

In Figure 35, the axial velocity profile along the centerline from the nozzle throat (x = 0) to the exit of the combustor is shown for two different time steps (50,000 and 90,000). The results are essentially the same for these two different instants, indicating that the URANS solution has reached the asymptotic steady state. Near the dump plane, the calculated values appreciably deviate from the experimentally determined mean value.

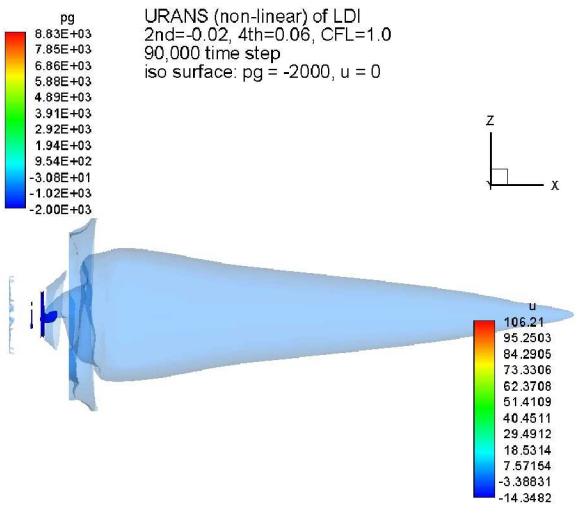

Figure 33.—PVC and VBB (side view).

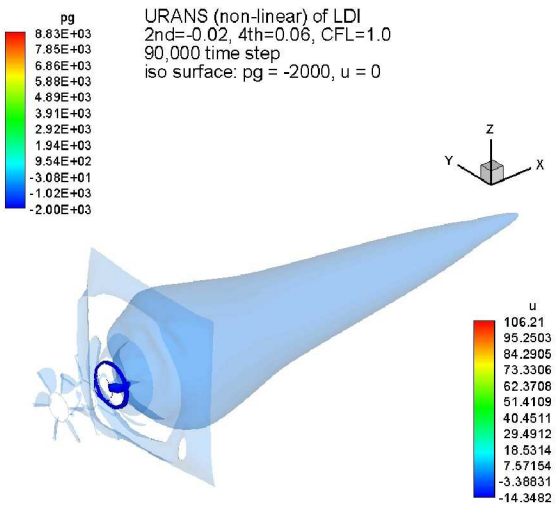

Figure 34.—PVC and VBB (a perspective view).

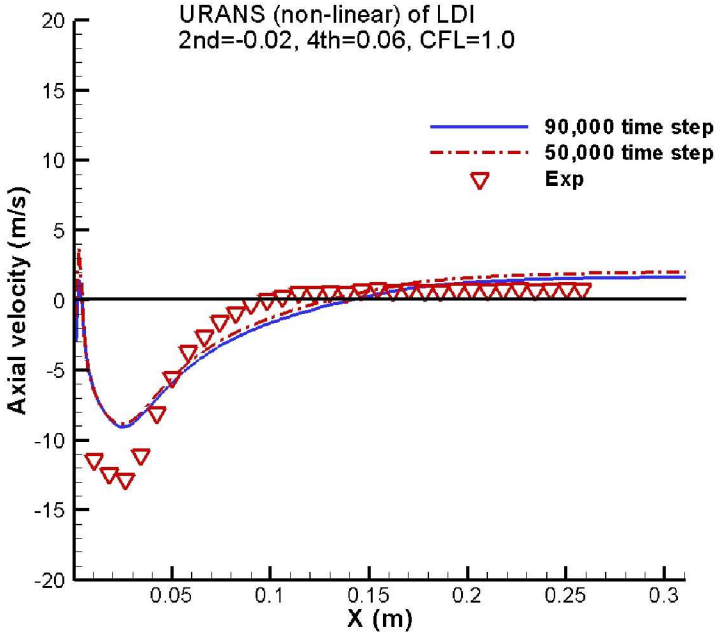

Figure 35.—Centerline axial velocity profile.

3.2.5 Distribution of Axial Velocity Along the y-axis at Downstream Locations

The distributions of the axial velocity along the y-axis (i.e., z = 0) at several downstream locations (x = 3, 6, 9, 12, 15, and 90 mm) are presented for two different time steps (50,000 and 90,000), they are also compared with the experimental mean values. Again, the differences between the numerical results at the 50,000 and the 90,000 time step are small. Figures 36 and 37 clearly indicate that, close to the dump plane, the calculated results and the experimental results do not agree well with each other. Further downstream, the agreement is reasonably well (Figs. 38 to 41).

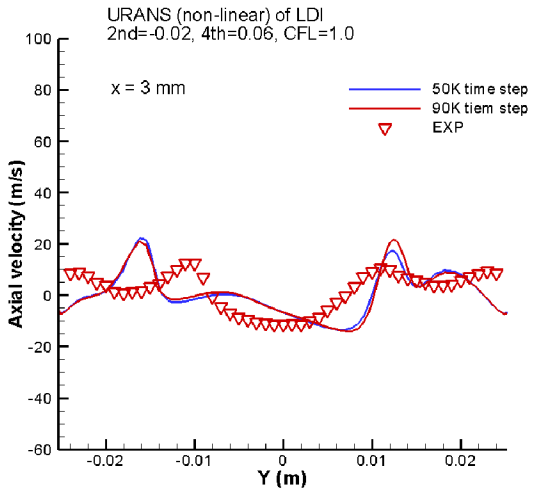

Figure 36.—Axial velocity at x = 3 mm.

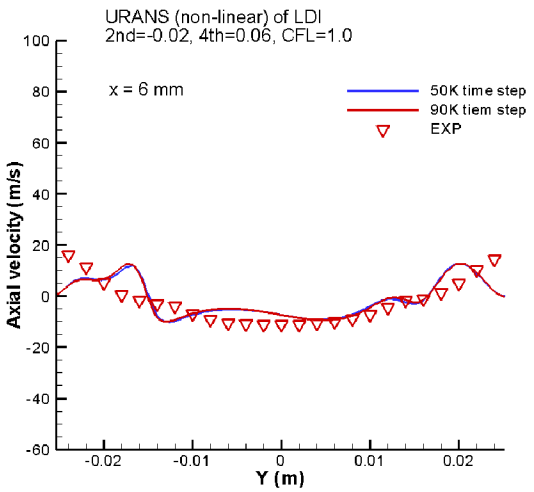

Figure 37.—Axial velocity at x = 6 mm.

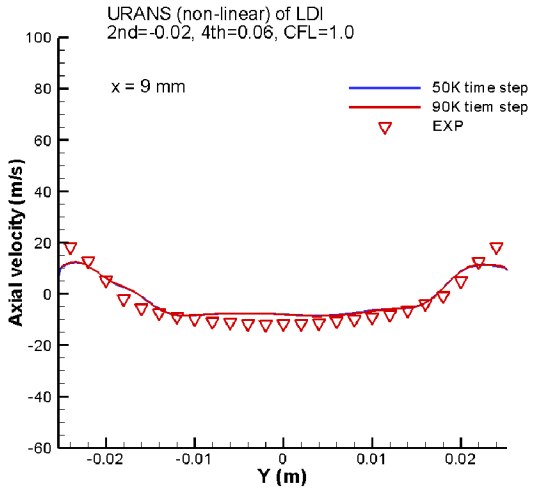

Figure 38.—Axial velocity at x = 9 mm.

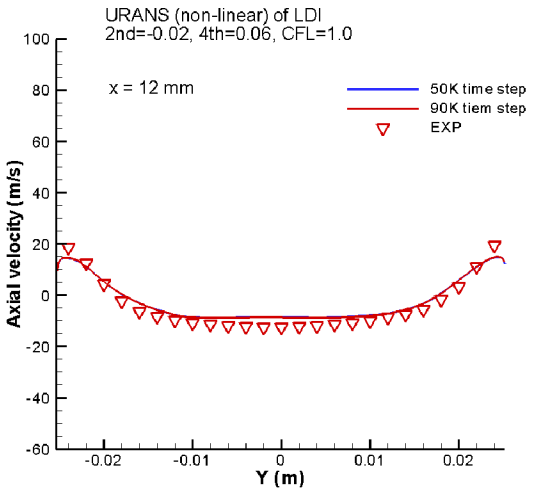

Figure 39.—Axial velocity at x = 12 mm.

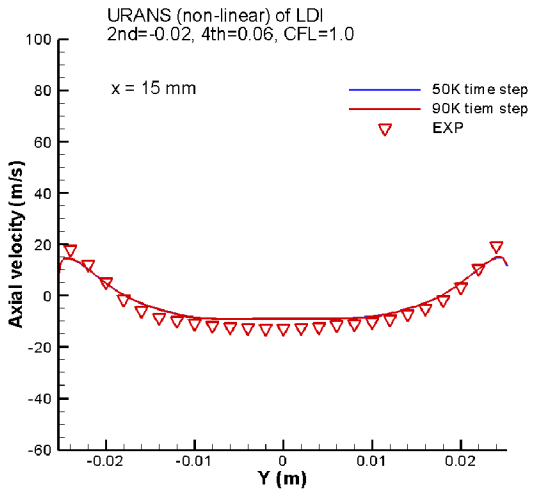

Figure 40.—Axial velocity at x = 15 mm.

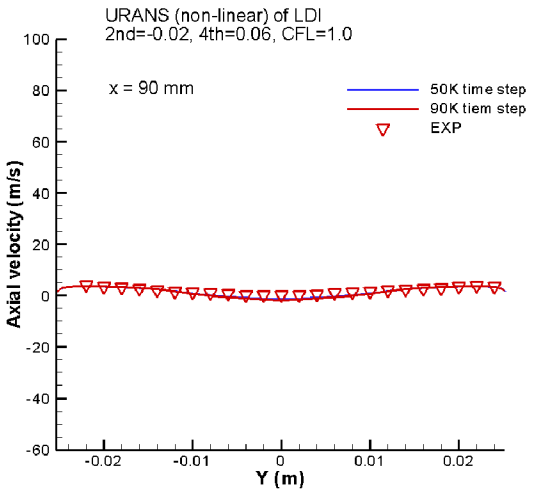

Figure 41.—Axial velocity at x = 90 mm.

3.2.6 Distribution of v, w Velocity Components Along the y-axis at Downstream Locations

The distributions of the other two velocity components v and w along the y-axis (i.e., z = 0) at several downstream locations (x = 3, 6, 9, 12, 15, and 90 mm) are presented for two different time steps (50,000 and 90,000). They also are compared with the experimental mean values. Again, the differences between the numerical results at the 50,000 and the 90,000 time steps are small. Figures 42 and 48 clearly indicate the appreciable disagreement between the URANS results and the experimental data. Figures 43 to 47 and 49 to 53 indicate that, further downstream, the agreement is reasonably good.

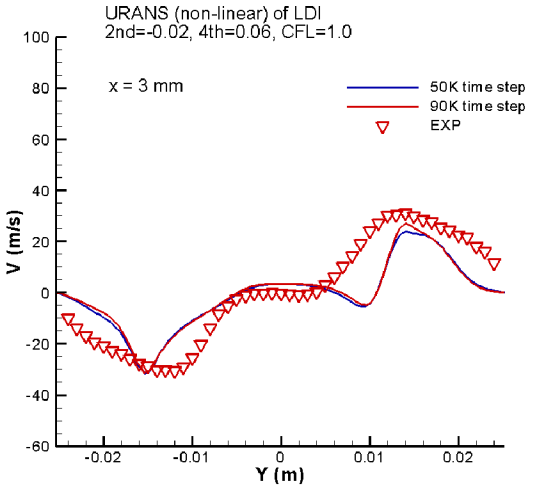

Figure 42.—Velocity component v at x = 3 mm.

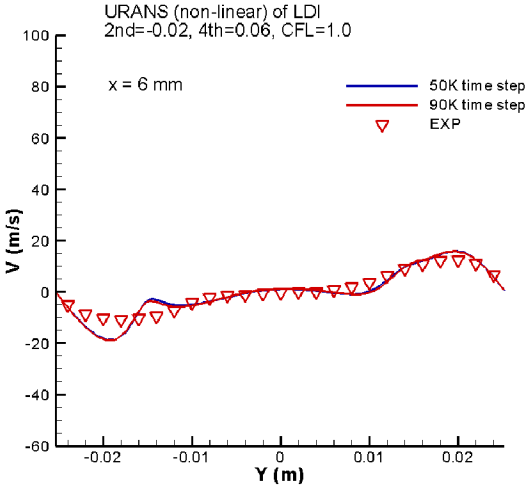

Figure 43.—Velocity component v at x = 6 mm.

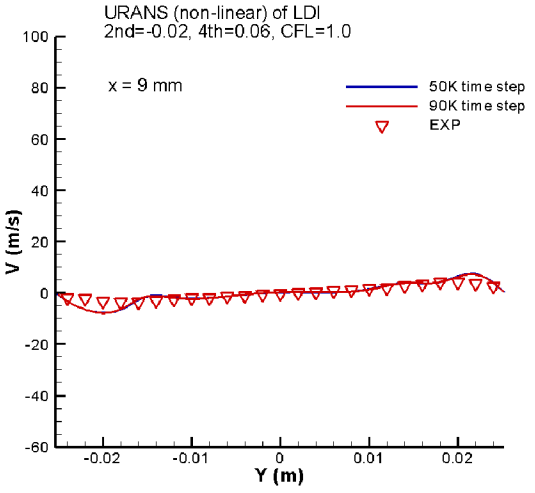

Figure 44.—Velocity component v at x = 9 mm.

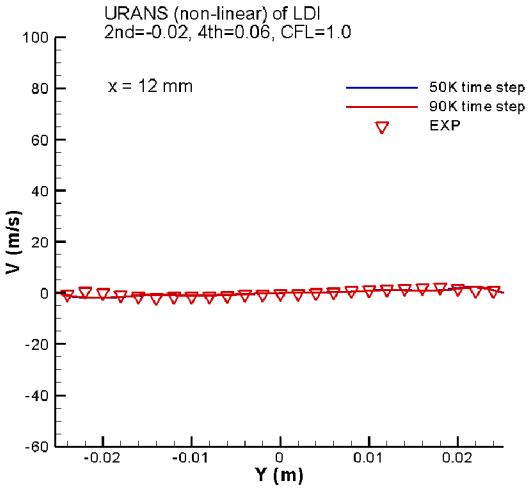

Figure 45.—Velocity component v at x = 12 mm.

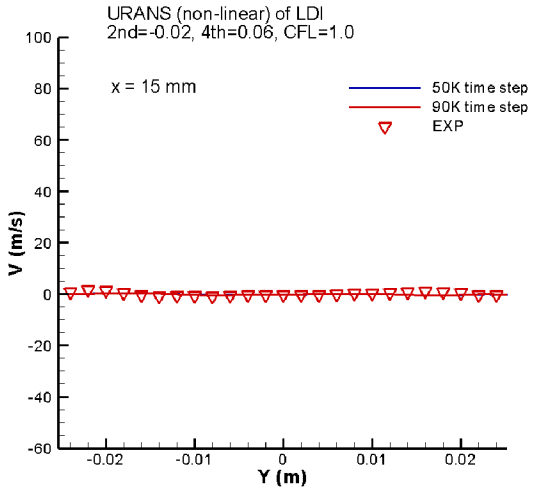

Figure 46.—Velocity component v at x = 15 mm.

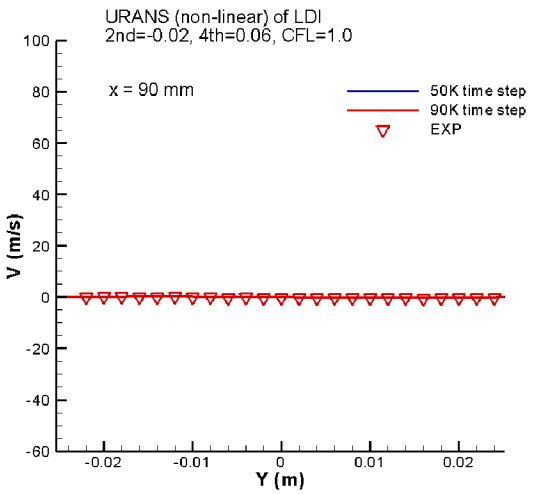

Figure 47.—Velocity component v at x = 90 mm.

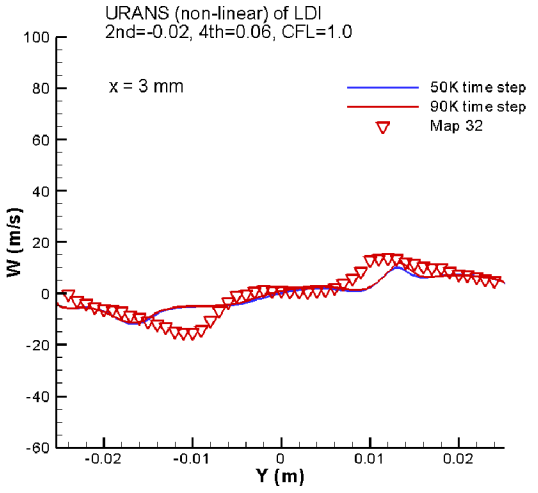

Figure 48.—Velocity component w at x = 3 mm.

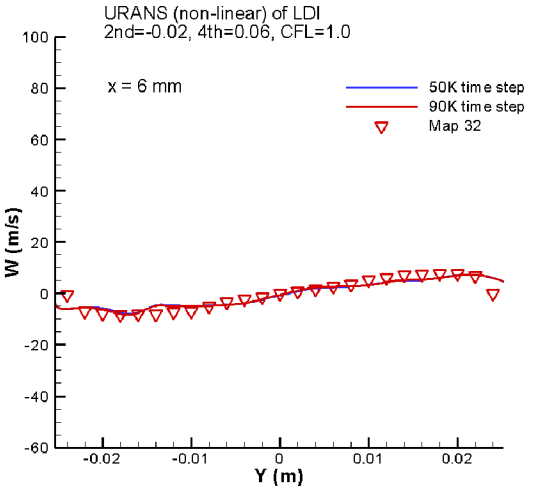

Figure 49.—Velocity component w at x = 6 mm.

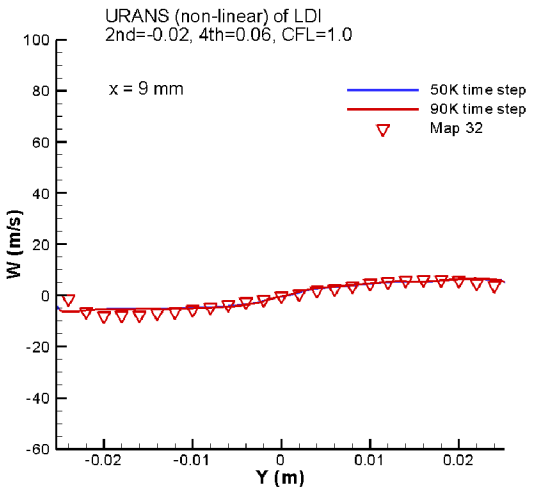

Figure 50.—Velocity component w at x = 9 mm.

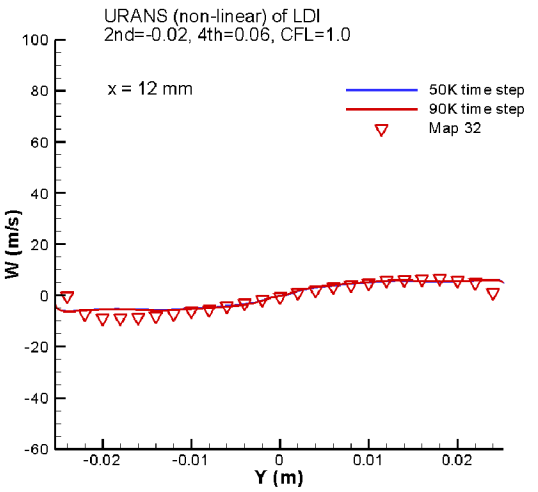

Figure 51.—Velocity component w at x = 12 mm.

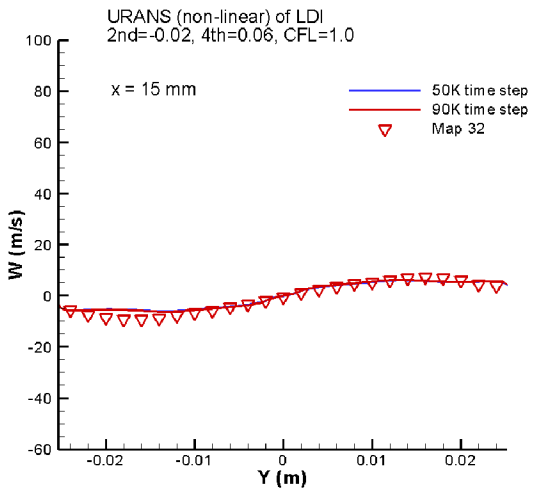

Figure 52.—Velocity component w at x = 15 mm

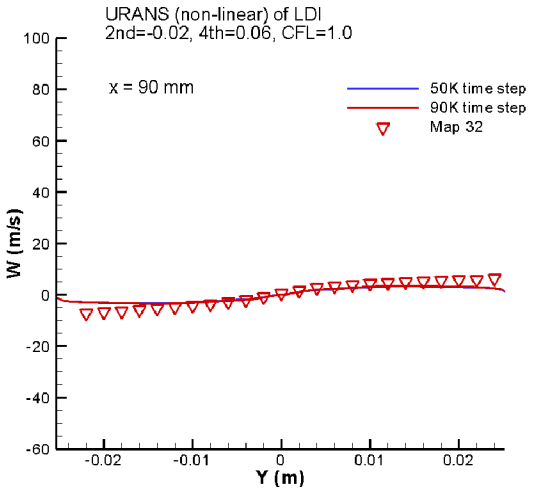

Figure 53.—Velocity component w at x = 90 mm.

3.3 Concluding Remarks

The URANS results presented above demonstrate that the steady solution of the mean turbulent flow exists. For URANS simulation, a larger numerical time step (10 times larger than the one used in PRNS/VLES) is adopted because, by its nature, it does not directly deal with the high frequency motions. The convergence order for the residuals of the pseudo time iteration is set to be one or one and half. This seems to be an optimal value, given the asymptotic convergence rate and the computing time consumed.

4.0 RANS of a Single-Element LDI Combustor

A steady RANS simulation has been carried out for a single-element LDI combustor to provide the initial flow field for performing the PRNS/VLES simulation presented in Section 2.0. The turbulence model is the nonlinear RANS model; the steady solution is obtained through a pseudo time iteration scheme, which is not time accurate.

4.1 Grid, Initial, and Boundary Conditions

The same computational domain and grid distribution shown in Figure 2 is used for the RANS simulation. At the inlet, the inflow velocity, the temperature and the density are specified. At the outflow boundary, the static pressure is imposed. The generalized wall function is applied to the solid wall boundaries. The initial condition is simply a static flow field.

4.2 Numerical Results

In the present RANS simulation, the following numerical parameters are set in the NCC code: the coefficient of the 2nd order dissipation = –0.01, the coefficient of the 4th order dissipation = 0.05, the initial gauge pressure pg = 0.0, the CFL number for the pseudo time iteration = 2.0, the tolerance for the mass imbalance = 1.0E-04, and all of the residual smoothing parameters are 0.0.

It takes about 150,000 iterations to reach the asymptotically converged state. Nevertheless, an additional 15,000 iterations are executed to insure that the specified mass imbalance tolerance is indeed met.

4.2.1 Contour Plots of Axial Velocity and Turbulent Kinetic Energy in the Center Plane

Figures 54 and 55 are the contours of the axial velocity u and the turbulent kinetic energy k in a center plane. They are the snapshots at the iteration number of 150,000. Figure 54 reveals a steady recirculation zone, which also extends into the upstream of the dump plane of the chamber. Figure 55 shows that higher turbulent kinetic energy k is concentrated in the diverging nozzle and near the dump plane. We also notice that the RANS value of the turbulent kinetic energy is about an order of magnitude higher than the instantaneous subscale turbulent kinetic energy from the PRNS/VLES simulation, as expected.

4.2.2 Contour Plots of Axial Velocity at the Combustor's Inlet and Outlet

Figure 56 is the contour of the axial velocity at the dump plane. Similar to the one predicted by the URANS simulation, it also reveals an asymmetric distribution of the axial velocity and a strong reverse flow off the center. Figure 57 is the contour of the axial velocity at the exit plane. A lower axial velocity region around the center is observed, which is typical for flows with swirling.

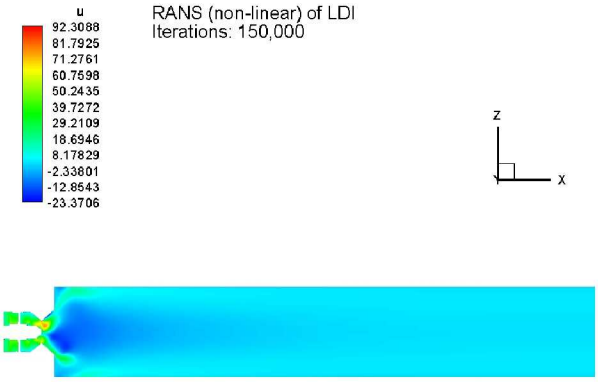

Figure 54.—Contour of axial velocity in center plane.

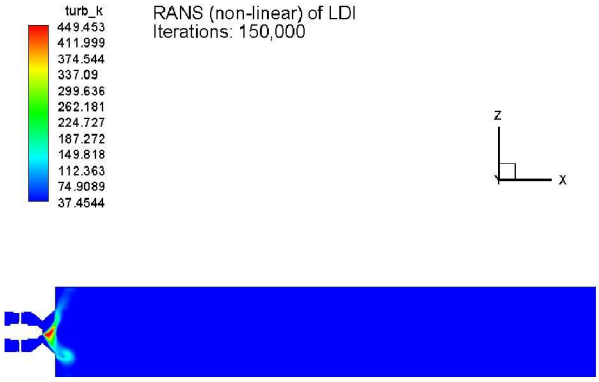

Figure 55.—Contour of k in center plane.

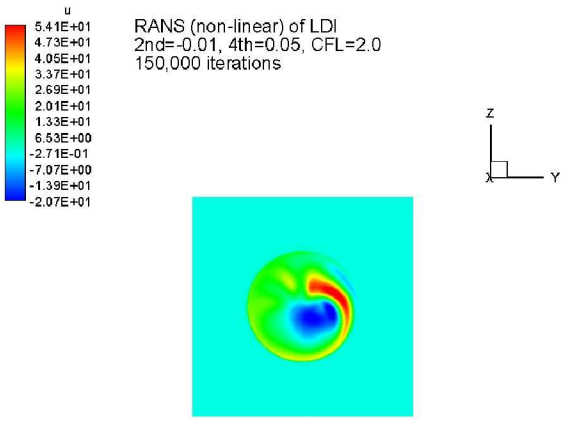

Figure 56.—Axial velocity at the dump plane.

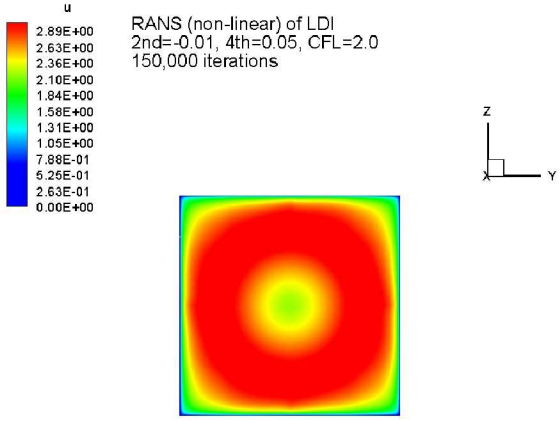

Figure 57.—Axial velocity at the exit plane.

4.2.3 PVC and VBB

For the purpose of comparing the characteristic flow structures captured by the RANS simulation with that captured by the PRNS/VLES or URANS simulations, we keep using the term PVC for the iso-surface of a relatively low pressure, and the term VBB for the iso-surface of the zero axial velocity, even now these RANS structures are time invariant. Figures 58 and 59 are the views from two different angles, one is the side view and the other is a perspective view. In these figures, the "PVC" is a short blue stick, its location and shape do not change with the time, and it does not line up with the centerline of the nozzle. This may explain why the distribution of the axial velocity at the dump plane is asymmetric. The VBB is the light green surface, which is quite smooth and, by and large, axisymmetric. It is the familiar central recirculation zone (CRZ).

4.2.4 Centerline Axial Velocity Profile

The axial velocity distribution along the centerline from the nozzle throat (x = 0) to the exit of the combustor at the iteration number 150,000 is compared with the experimental mean data (Fig. 60). The agreement is reasonable.

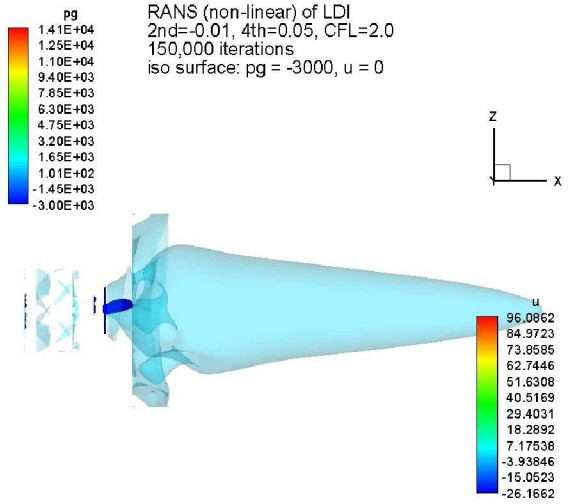

Figure 58.—PVC and VBB (side view).

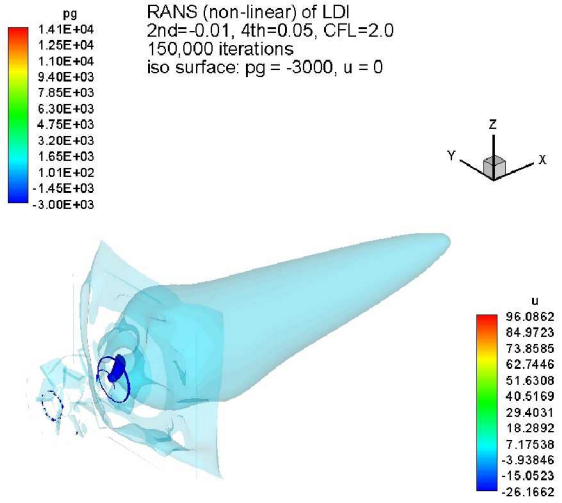

Figure 59.—PVC and VBB (a perspective view).

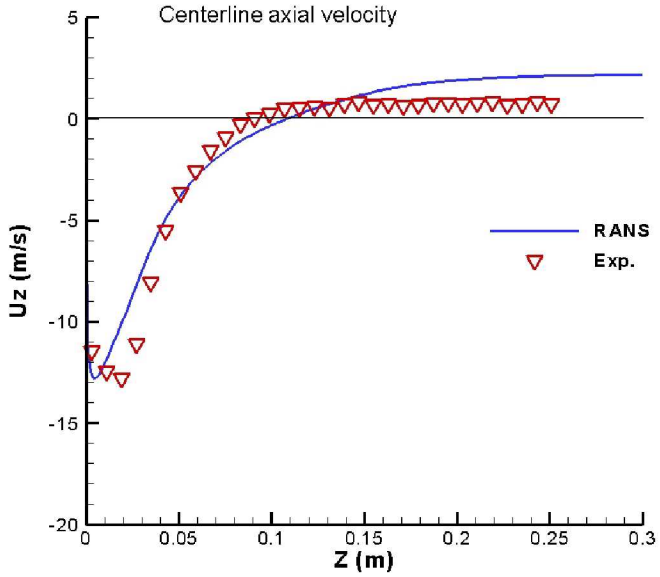

Figure 60.—Centerline axial velocity profile.

4.2.5 Distribution of Axial Velocity Along the y-axis at Downstream Locations

The distributions of the axial velocity along the y-axis (i.e., z = 0) at several downstream locations (x = 3, 6, 9, 12, 15, and 90 mm) are presented for the iteration number 150,000, also included are the experimentally determined mean values. Figures 61 and 62 clearly indicate the mismatching between the RANS results and the experimental data. Further downstream, the agreements become reasonable (Figs. 63 to 66).

4.2.6 Distribution of v, w Velocity Components Along the y-axis at Downstream Locations

The distributions of the other two velocity components v and w along the y-axis (i.e., z = 0) at several downstream locations (x = 3, 6, 9, 12, 15, and 90 mm) are presented for the iteration number 150,000, also included are the experimentally determined mean values. Figures 67 and 73 clearly indicate the mismatching between the RANS results and the experimental data, the agreement become reasonable in further downstream (Figs. 68 to 72 and 74 to 78).

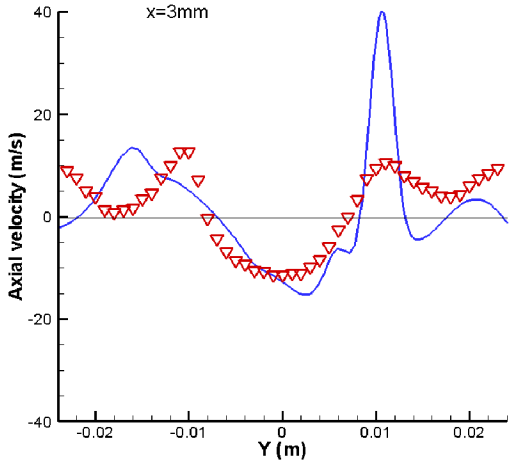

Figure 61.—Axial velocity at x = 3 mm.

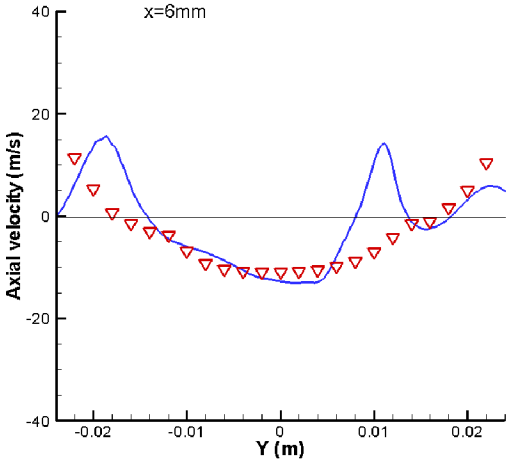

Figure 62.—Axial velocity at x = 6 mm.

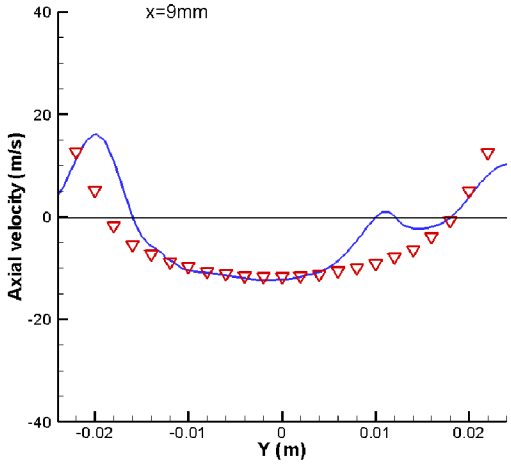

Figure 63.—Axial velocity at x = 9 mm.

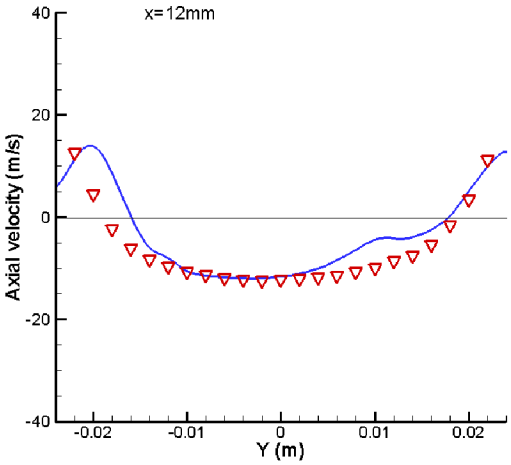

Figure 64.—Axial velocity at x = 12 mm.

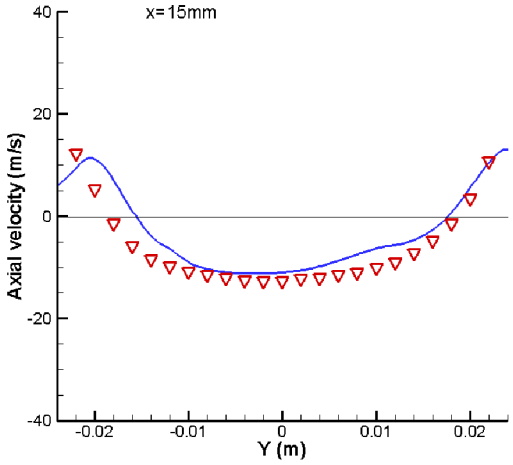

Figure 65.—Axial velocity at x = 15 mm.

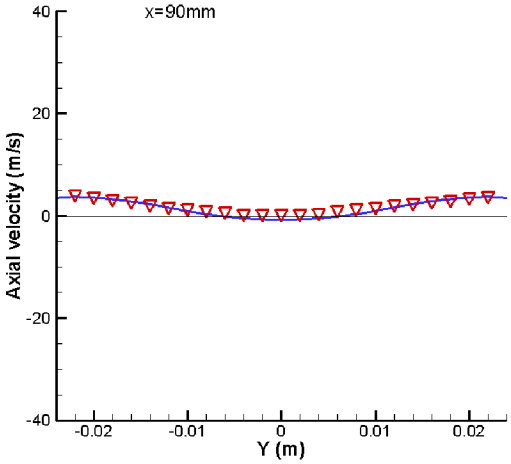

Figure 66.—Axial velocity at x = 90 mm.

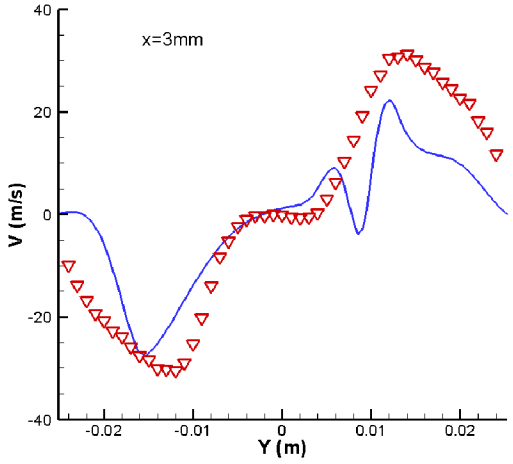

Figure 67.—Velocity component v at x = 3 mm.

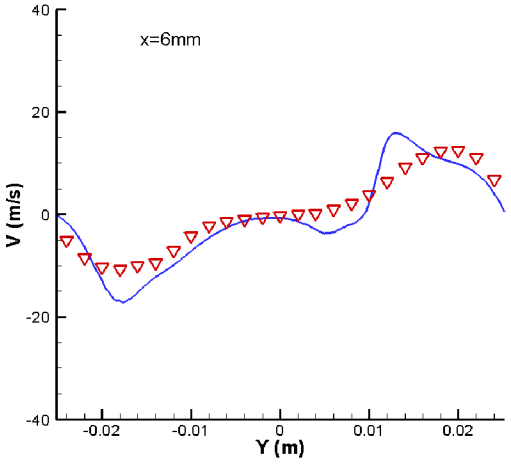

Figure 68.—Velocity component v at x = 6 mm.

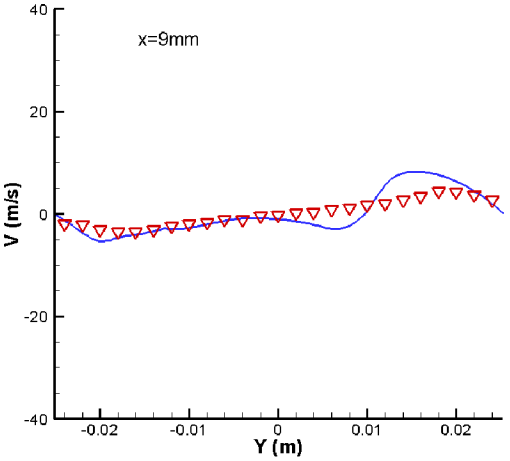

Figure 69.—Velocity component v at x = 9 mm.

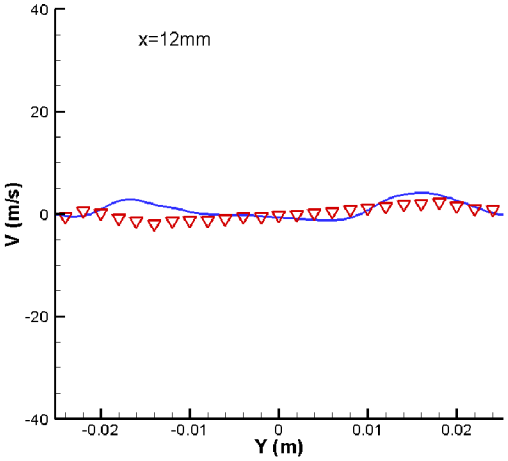

Figure 70.—Velocity component v at x = 12 mm.

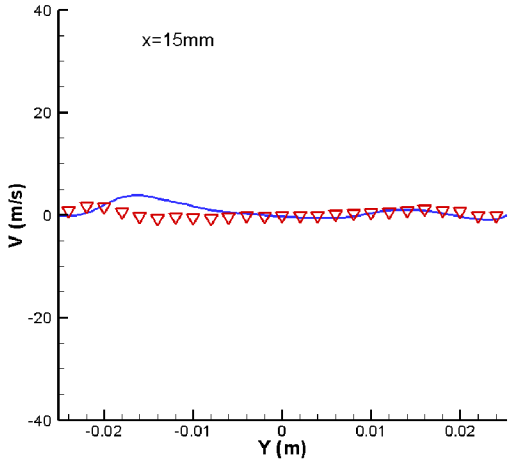

Figure 71.—Velocity component v at x = 15 mm.

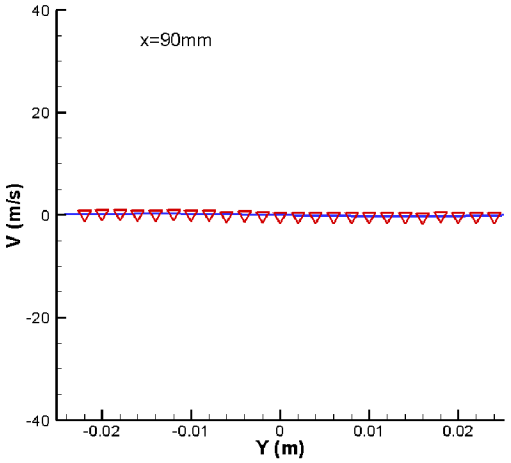

Figure 72.—Velocity component v at x = 90 mm.

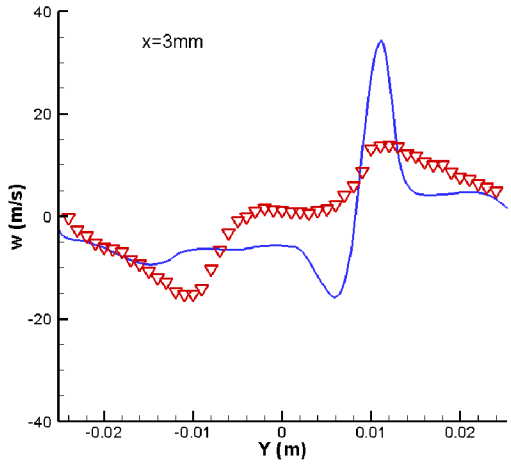

Figure 73.—Velocity component w at x = 3 mm.

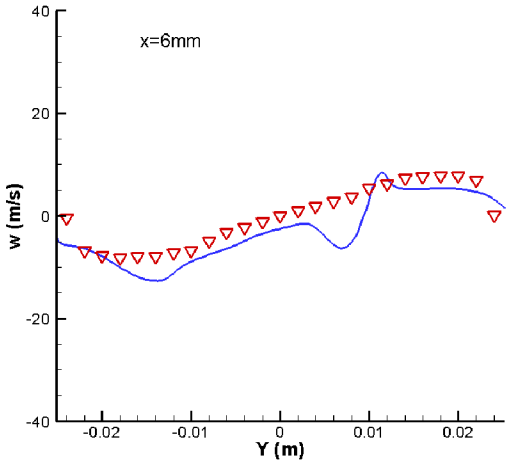

Figure 74.—Velocity component w at x = 6 mm.

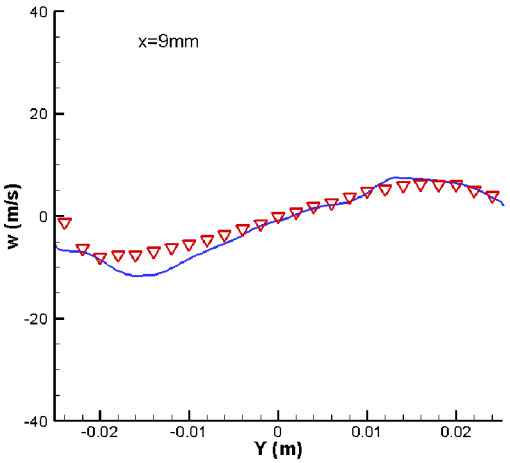

Figure 75.—Velocity component w at x = 9 mm.

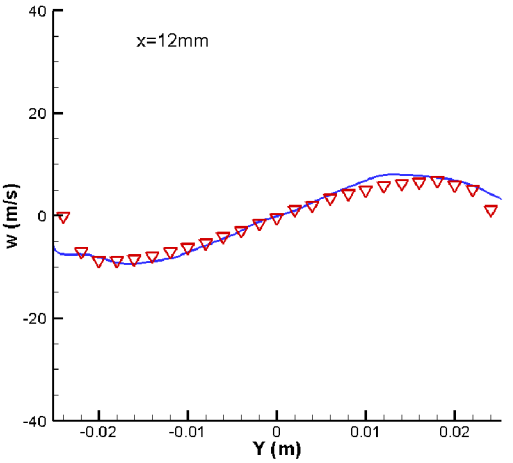

Figure 76.—Velocity component w at x = 12 mm.

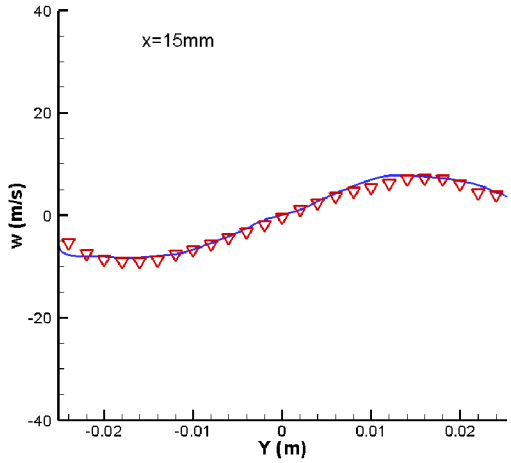

Figure 77.—Velocity component w at x = 15 mm.

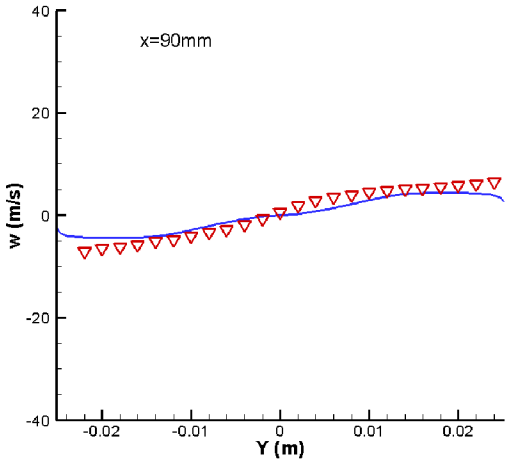

Figure 78.—Velocity component w at x = 90 mm.

4.3 Concluding Remarks

The RANS simulation is performed to provide an initial condition for the PRNS/VLES simulation presented in Section 2.0. Nevertheless, the RANS results presented in this section indicate that the steady solution is quite meaningful when comparing with the experimental mean values, except for some mismatching near the dump plane of the combustion chamber. The unsteady PVC and VBB turbulent structures observed in PRNS/VLES are now degenerated into a steady, short vortex core and a steady, center recirculation zone; respectively. The level of the turbulent kinetic energy predicted by the present RANS simulation is consistent with our expectation, which is about an order of magnitude larger than the subscale turbulent kinetic energy predicted by PRNS/VLES. The steady RANS solution is obtained with a CPU time which is about 15 to 20 times less than the CPU time required by PRNS/VLES or URANS (assuming the number of time steps run is 45,000 to 60,000).

It is noted here that the convergence criterion for reaching the steady RANS solution is the specified tolerance of the mass imbalance. In the present RANS simulation, we have observed that, after a certain number of pseudo iterations, the residual level reaches a plateau, and the value of the residual is only reduced by about 50 percent, when compared with its initial value. This is far from the two or three orders of magnitude reduction obtained in the PRNS/VLES simulation. The reason for this problem is under investigation. One possibility is the attempt of using a steady approach to simulate a flow which contains intrinsically unsteady, large scale structures. However, for the purpose of providing an initial condition for PRNS/VLES, the present RANS simulation should be adequate.

5.0 Summary

Numerical simulations of the non-reacting flow in a single-element LDI combustor have been carried out using the RANS, URANS and PRNS/VLES approaches and the same computational domain and grid distribution.

The steady RANS solution is used as the initial condition for the PRNS/VLES simulation. The URANS simulation is performed to explore whether or not appreciable unsteadiness exist in the turbulent mean flow. The answer is no for the present case, because the URNAS simulation evolves towards a steady state.

The PRNS/VLES simulation using a nonlinear subscale model has been successfully carried out. The numerical results are in reasonable agreement with the experimental data. They also have clearly revealed the dynamically important large scale turbulent structures occurring in the LDI configurations: the precessing vortex core (PVC) and the vortex breaks down bubble (VBB). These results have

demonstrated that the PRNS/VLES approach with the nonlinear subscale model is capable of capturing the large or very large turbulent flow structures with a RANS type of grid.

The present study suggests that, for a turbulent flow in a complex geometry, it is worthwhile to conduct the RANS simulation, because it can relatively quickly generate a global view of the mean field of the turbulent flow. In many cases, this is probably sufficient for the application in mind. However, if the flow itself clearly exhibits large scale unsteadiness, and/or mixing process is of major interest, then we must further carry out the PRNS/VLES using the RANS solution as the initial condition.

References

1. Liu, N.-S., and Shih, T.-H., "Turbulence Modeling for Very Large-Eddy Simulation," *AIAA Journal,* vol. 44, no. 4, 2006, pp. 687–697.
2. Shih, T.-H., and Liu, N.-S., "Modeling of Internal Reacting Flows and External Static Stall Flows Using RANS and PRNS," Flow, Turbulence and Combust (2008) 81:279–299.
3. Shih, T.-H. and Liu, N.-S., "Assessment of the Partially Resolved Numerical Simulation (PRNS) Approach in the National Combustion Code (NCC) for Turbulent Nonreacting and Reacting Flows," NASA/TM—2008-215418.
4. Shih, T.-H. and Liu, N.-S., "Numerical Study of Outlet Boundary Conditions for Unsteady Turbulent Internal Flows Using the NCC," NASA/TM—2009-215486.
5. Shih, T.-H. and Liu, N.-S., "A Nonlinear Dynamic Subscale Model for PRNS/VLES of Internal Combustor Flows," AIAA–2009–0467, January 4 to 8, 2009, Orlando, FL.
6. Davoudzadeh, F., Liu, N.-S. and Moder, J.P., "Investigation of Swiring Air Flows Generated by Axial Swirlers in a Flame Tube," Proceedings of GT2006 ASME Turbo Expo 2006: Power for Land, Sea, and Air May 8–11, 2006, Barcelona, Spain.
7. Cai, J., Jeng, S.-M., and Tacina, R., "The Structure of A Swirl-Stablized Reacting Spray Issued From an Axial Swirler," AIAA–2005–1424, 43rd AIAA Aerospace Science Meeting and Exhibit, 10–13 January 2005, Reno, NV.
8. Shih, T.-H., Povinelli, L.A., and Liu, N.-S., "Application of Generalized Wall Function for Complex Turbulent Flows," J. of Turbulence, 4 (2003) 015.
9. Quealy, A., Ryder, R.C., Norris, A.T., and Liu, N.-S., "National Combustion Code: Parallel Implementation and Performance," AIAA Paper 2000–0336, 2000.
10. Patel, N. Suresh, M., "Simulation of Spray-Turbulence-Flame Interactions in a Lean Direct Injection Combustor," Combustor and Flame 153 (2008) 228–257.

REPORT DOCUMENTATION PAGE		Form Approved OMB No. 0704-0188

1. REPORT DATE *(DD-MM-YYYY)*	2. REPORT TYPE	3. DATES COVERED *(From - To)*
01-08-2009	Technical Memorandum	

4. TITLE AND SUBTITLE
A Very Large Eddy Simulation of the Nonreacting Flow in a Single-Element Lean Direct Injection Combustor Using PRNS With a Nonlinear Subscale Model

5a. CONTRACT NUMBER

5b. GRANT NUMBER

5c. PROGRAM ELEMENT NUMBER

6. AUTHOR(S)
Shih, Tsan-Hsing; Liu, Nan-Suey

5d. PROJECT NUMBER

5e. TASK NUMBER

5f. WORK UNIT NUMBER
WBS 561581.02.08.03.16.02

7. PERFORMING ORGANIZATION NAME(S) AND ADDRESS(ES)
National Aeronautics and Space Administration
John H. Glenn Research Center at Lewis Field
Cleveland, Ohio 44135-3191

8. PERFORMING ORGANIZATION REPORT NUMBER
E-16956

9. SPONSORING/MONITORING AGENCY NAME(S) AND ADDRESS(ES)
National Aeronautics and Space Administration
Washington, DC 20546-0001

10. SPONSORING/MONITOR'S ACRONYM(S)
NASA

11. SPONSORING/MONITORING REPORT NUMBER
NASA/TM-2009-215644

12. DISTRIBUTION/AVAILABILITY STATEMENT
Unclassified-Unlimited
Subject Categories: 01 and 64
Available electronically at http://gltrs.grc.nasa.gov
This publication is available from the NASA Center for AeroSpace Information, 443-757-5802

13. SUPPLEMENTARY NOTES

14. ABSTRACT
Very large eddy simulation (VLES) of the nonreacting turbulent flow in a single-element lean direct injection (LDI) combustor has been successfully performed via the approach known as the partially resolved numerical simulation (PRNS/VLES) using a nonlinear subscale model. The grid is the same as the one used in a previous RANS simulation, which was considered as too coarse for a traditional LES simulation. In this study, we first carry out a steady RANS simulation to provide the initial flow field for the subsequent PRNS/VLES simulation. We have also carried out an unsteady RANS (URANS) simulation for the purpose of comparing its results with that of the PRNS/VLES simulation. In addition, these calculated results are compared with the experimental data. The present effort has demonstrated that the PRNS/VLES approach, while using a RANS type of grid, is able to reveal the dynamically important, unsteady large-scale turbulent structures occurring in the flow field of a single-element LDI combustor. The interactions of these coherent structures play a critical role in the dispersion of the fuel, hence, the mixing between the fuel and the oxidizer in a combustor.

15. SUBJECT TERMS
Injector; Very large eddy simulation; CFD

16. SECURITY CLASSIFICATION OF:			17. LIMITATION OF ABSTRACT	18. NUMBER OF PAGES	19a. NAME OF RESPONSIBLE PERSON
a. REPORT	b. ABSTRACT	c. THIS PAGE			STI Help Desk (email:help@sti.nasa.gov)
U	U	U	UU	29	19b. TELEPHONE NUMBER *(Include area code)* 443-757-5802